# Eight-Unit-Cell Electronic Modulations in Cuprates Originating from Local Molecular Orbitals

Zhiheng Yao,[1,*] Sixuan Chen,[1,*] Jianfa Zhao,[2,*] Shusen Ye,[1] Weixiang Qu,[1] Ning Xia,[1] Yuling Dai,[2] Luchuan Shi,[2] Hongrui Zhang,[1] Zhenqi Hao,[1] Changqing Jin,[2] Shuo Yang,[1,3,4,†] and Yayu Wang[1,3,4,‡]

[1]*State Key Laboratory of Low Dimensional Quantum Physics, Department of Physics, Tsinghua University, Beijing 100084, China*
[2]*Beijing National Laboratory for Condensed Matter Physics, Institute of Physics, Chinese Academy of Sciences, Beijing 100190, China*
[3]*New Cornerstone Science Laboratory, Frontier Science Center for Quantum Information, Beijing 100084, China*
[4]*Hefei National Laboratory, Hefei 230088, China*

(Received 10 March 2026; accepted 3 September 2026; published 5 October 2026)

The pair density wave state with eight-unit-cell ($8a_0$) periodicity has been widely regarded as the primary order in cuprates, yet its existence and origin remain subjects of intense debate. Using spectroscopic imaging scanning tunneling microscopy, we observe spatial modulations of the electronic states with approximately $8a_0$ periodicity in both the superconducting and insulating regimes of hole-doped $Ca_2CuO_2Cl_2$ cuprate. We find that the $8a_0$ spatial patterns are generated by the formation of molecular orbitals by doped holes, which organize into $4a_0 \times 4a_0$ plaquettes as the basic unit. Our results identify the $4a_0$ molecular-orbital plaquette as the fundamental electronic building block in cuprates, while the $8a_0$ pair density wave represents a spatial subharmonic that emerges at sufficiently high doping.

DOI: 10.1103/lvpn-gblk

The pair density wave (PDW) can be generally described as a superconducting state in which the Cooper pairing exhibits periodic oscillations in real space and carries a net momentum in $k$ space [1–3]. The PDW has long been conjectured theoretically to be a primary order [4–6] behind various anomalous phenomena in cuprates [7–12]. In recent years, scanning probe techniques have directly visualized the PDW state in cuprates, igniting intense interest [13–17]. In particular, scanning tunneling microscopy (STM) on optimally doped $Bi_2Sr_2CaCu_2O_{8+\delta}$ (Bi-2212) revealed a modulation with eight-unit-cell ($8a_0$) periodicity within vortex halos induced by external magnetic field [15]. Scanning Josephson tunneling microscopy, utilizing a Bi-2212 flake as superconducting tip, discovered an $8a_0$ modulation in the gap map without external magnetic field, which is considered compelling evidence for PDWs [16].

Despite these advances, heated debates persist regarding the nature of the $8a_0$ PDW. First, is the PDW a long-range density wave order or is it better characterized as short-range modulations? Although the Fourier transform (FT) gap map does reveal a $2\pi/8a_0$ wave vector, pinpointing the corresponding long-range order in real space has been difficult, with only sporadic features showing roughly $8a_0$ spacing. Second, is it the primary order driving all other phases, as suggested by many theories, or a subsidiary feature derived from another order? There are reports of PDWs with the same $4a_0$ checkerboard periodicity [13,14,17], but the search for their secondary charge order by scattering probes has been fruitless. Third, how does a PDW emerge upon doping the parent Mott insulator? All prior PDW experiments on cuprates were performed near optimal doping; however, to reveal its origin, it is crucial to investigate the severely underdoped regime where pairing just starts to emerge.

To address these critical issues, in this Letter we use STM to investigate alkali-metal-doped $Ca_2CuO_2Cl_2$ (CCOC) with varied hole densities across the insulator-superconductor phase boundary. We directly detect the $8a_0$ modulations in the differential conductance ($dI/dV$) maps in both the superconducting and insulating samples. The primary spatial patterns, including the $8a_0$ periodicity and low-energy unidirectional order, can be explained by the formation of molecular orbital framework with $4a_0 \times 4a_0$ plaquette as the basic unit. The "molecular orbitals" refer to the spatially extended electronic states formed by the overlap of atomic orbitals of doped holes, as established in our previous work [18]. These molecular-orbital states manifest as $4a_0$ plaquettes with internal stripelike features at low energy and ladderlike features at high energy in the $dI/dV$ maps, as detailed in Supplemental Material Sec. I [19]. We propose that the $8a_0$ modulation represents a spatial subharmonic of the $4a_0$ molecular orbital patterns, possessing a real-space origin distinctively different from a PDW order arising from finite momentum pairing.

We begin with a superconducting CCOC with hole density $p = 0.10$ and $T_c = 14$ K. The electrochemically etched tungsten tip was carefully treated and calibrated

*These authors contributed equally to this work.
†Contact author: shuoyang@tsinghua.edu.cn
‡Contact author: yayuwang@tsinghua.edu.cn

 © 2026 American Physical Society

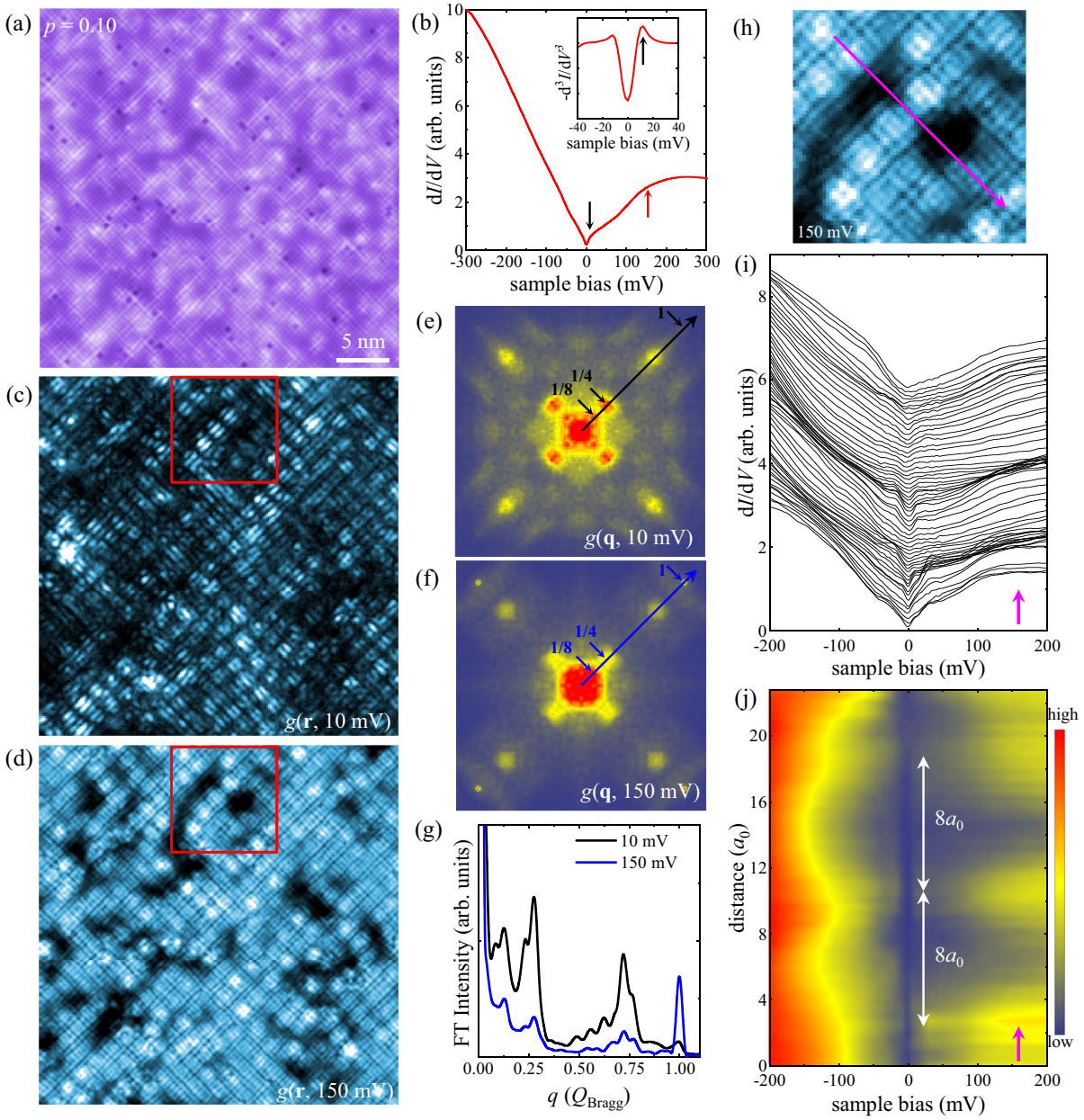



FIG. 1. Eight-unit-cell modulation in the superconducting $p = 0.10$ sample. (a) Large-scale topographic image of the $p = 0.10$ sample acquired at $T = 5$ K. (b) Spatially averaged $\mathrm{d}I/\mathrm{d}V$ spectrum showing the superconducting gap and pseudogap. The inset is the $-\mathrm{d}^3I/\mathrm{d}V^3$ curve from $-40$ to 40 mV, where the superconducting gap can be clearly resolved. (c),(d) $\mathrm{d}I/\mathrm{d}V$ maps at bias $V_b = 10$ and 150 mV. (e),(f) FT maps of (c) and (d), revealing peaks at $q \approx 1/4$ and $q \approx 1/8$. (g) Line profiles along the Cu-O bond directions in (e) and (f), highlighting both wave vectors. (h) Enlargement of the red square in (c) and (d). (i),(j) $\mathrm{d}I/\mathrm{d}V$ spectra and color plot along the magenta arrow in (h), showing clear $8a_0$ modulations that persist across a large energy range.

prior to the measurements to ensure stable and reliable spectroscopic performance [23]. A large-area topography is shown in Fig. 1(a), and the spatially averaged $\mathrm{d}I/\mathrm{d}V$ spectrum in Fig. 1(b) exhibits a superconducting gap with size around 10 meV (black arrow) and a pseudogap around 150 meV (red arrow). The superconducting gap feature is more clearly revealed by the $-\mathrm{d}^3I/\mathrm{d}V^3$ curve in the inset. The pseudogap size of ~150 meV is estimated from the energy scale below which the spectral weight is strongly suppressed [24], and the fitting details are provided in Supplemental Material Sec. II [19]. The $\mathrm{d}I/\mathrm{d}V$ maps at these two characteristic energies are shown in Figs. 1(c) and 1(d), where stripe- and ladder-shaped molecular orbital patterns dominate the field of view (FOV), interrupted only by a small number of dark pits induced by the voids in the molecular-orbital plaquette network. FT analysis of the $\mathrm{d}I/\mathrm{d}V$ maps shown in Figs. 1(e) and 1(f) reveals pronounced peaks at $q \approx 1/4$ and $q \approx 1/8$ (in units of $2\pi/a_0$)

along the line profiles taken along the Cu-O bond direction in Fig. 1(g), corresponding to real-space modulations with $4a_0$ and $8a_0$ periodicities. The $q \approx 1/4$ peak is attributed to the periodic order of plaquettes with size around $4a_0 \times 4a_0$, a feature well-established in previous reports on the checkerboard phase [18,25–33].

The observed $8a_0$ modulation matches the periodicity of the PDW in optimally doped Bi-2212 [16]. Unlike the prior Josephson-tunneling study that requires a superconducting tip, here the $8a_0$ modulation is directly resolved in $\mathrm{d}I/\mathrm{d}V$ maps using a normal metal tip. To further examine its relationship with superconductivity, we analyze spatial maps of superconductivity-related quantities in Supplemental Material Sec. III [19]. Pronounced signatures of the $8a_0$ modulation are obtained from both the gap depth $[H = \mathrm{d}I/\mathrm{d}V(V_{\mathrm{SC}}) - \mathrm{d}I/\mathrm{d}V(0)]$ and sharpness $[D = -\mathrm{d}^3I/\mathrm{d}V^3(V_{\mathrm{SC}})]$ maps. The consistent presence of the $8a_0$ modulation across these quantities establishes it as an intrinsic modulation of the local pairing amplitude.

To reveal the origin of the $8a_0$ modulation, Fig. 1(i) displays a series of $\mathrm{d}I/\mathrm{d}V$ spectra taken along the magenta arrow in Fig. 1(h), which crosses two dark pits in the $\mathrm{d}I/\mathrm{d}V$ map at $V_{\mathrm{b}} = 150$ mV. All $\mathrm{d}I/\mathrm{d}V$ spectra exhibit characteristic V-shaped gaps, whose depth and sharpness oscillate periodically along the linecut. The corresponding color plot in Fig. 1(j) reveals a clear $8a_0$ modulation, where the locations with small $\mathrm{d}I/\mathrm{d}V$ values correspond to the two dark pits. This modulation thus originates from the approximately $4a_0$ lateral extent of the dark pits separating the plaquettes also with a typical $4a_0$ size. Real-space masking and momentum-space filtering analyses in Supplemental Material Sec. IV [19] corroborate the dominant contribution of these dark pits to the observed $8a_0$ Fourier component. Figures 1(i) and 1(j) also demonstrate that the $8a_0$ modulation persists over a large energy range far beyond the superconducting gap. Therefore, it is not merely a PDW, but instead a universal modulation of the overall electronic states. This $8a_0$ modulation is also observed on another FOV of the same sample (Supplemental Material Sec. V [19]).

Previous works in underdoped $Bi_2Sr_2CuO_{6+\delta}$ (Bi-2201) and CCOC have revealed that each $4a_0 \times 4a_0$ plaquette accommodates two doped holes on average [18,34,35]. In Supplemental Material Sec. VI [19], we show that the results reported here are consistent with this conclusion. At a nominal doping of $p = 1/8$, a uniform distribution of doped holes would yield a dense tiling of such $4a_0$ plaquettes covering the whole FOV. At lower doping, such as $p = 0.10$ here, incomplete plaquette coverage inevitably produces dark pits. Our data demonstrate that the depletion of electronic states also occurs in the unit of an entire plaquette, which creates dark pits with size around $4a_0$. This observation further strengthens our statement that the $4a_0 \times 4a_0$ plaquette is the fundamental building block for electronic states in cuprates [18].

We then examine an underdoped insulating CCOC with doping level $p = 0.05$. The $\mathrm{d}I/\mathrm{d}V$ maps acquired at 30 and 200 mV are presented in Figs. 2(a) and 2(b). Compared to the $p = 0.10$ case, this sample contains larger dark pits devoid of doped holes, reflecting the more dilute dopant distribution. The red box in Figs. 2(a) and 2(b) highlights a representative region with elongated plaquette chains separated by a characteristic distance around $4a_0$. A closer inspection reveals that two neighboring chains are bridged by a $4a_0$ plaquette at one end, resulting in an empty channel between them with distance around $4a_0$. These chains typically extend for 3–5 plaquettes, with the internal stripes at low energy preferentially aligned along the same direction [18]. Together with the $4a_0$ size of each plaquette, this unique configuration generates a robust, unidirectional $8a_0$ modulation perpendicular to the chain direction.

Our previous work has established that the stripe- and ladder-shaped electronic states are derived from the molecular orbitals formed by two holes on neighboring alkali dopants [18]. Although the specific structure of molecular orbitals varies with energy [35–37]—consistent with the form factor in both STM and x-ray experiments [38–41]—the spatial arrangement of the $4a_0$ plaquettes remains robust. This invariance explains the persistence of the $8a_0$ modulation across a wide energy range. To directly visualize this robustness, we present spectra and the corresponding color plot [Figs. 2(c) and 2(d)] taken along the red linecut in Figs. 2(a) and 2(b). These data reveal an $8a_0$ modulation spanning three periods over a large energy window, similar to that observed in the superconducting sample. Notably, the spectra here exhibit U-shaped gaps, in contrast to the V-shaped gap characteristic of $d$-wave superconductivity. This observation indicates that the $8a_0$ modulation is not tightly bound to well-defined $d$-wave pairing. Instead, it represents a preexisting electronic texture of the molecular-orbital plaquette network. With increasing doping level hence the coverage of plaquettes, superconductivity develops on top of the electronic modulations, leading to the $8a_0$ spatial modulations of superconducting properties.

More importantly, the internal structure of plaquettes plays a crucial role in determining how they assemble into $8a_0$ modulations. The $\mathrm{d}I/\mathrm{d}V$ map acquired at 30 mV from another FOV in the $p = 0.05$ sample [Fig. 2(e)] reveals long, well-aligned chains separated by approximately $4a_0$ channels, resulting in a nearly unidirectional $8a_0$ modulation [Fig. 2(f)]. The magenta linecut across these chains in Fig. 2(g) shows that the $8a_0$ modulation coexists with the internal stripe features within each plaquette. As previously reported [18,35], the internal stripes of adjacent plaquettes tend to align along the chain direction, as a result of molecular-orbital formation. Since the $8a_0$ modulation arises from the separation between plaquette chains, its direction is strongly correlated with the orientation of the internal stripes, as evidenced in Figs. 1(c), 2(a), and 2(e).

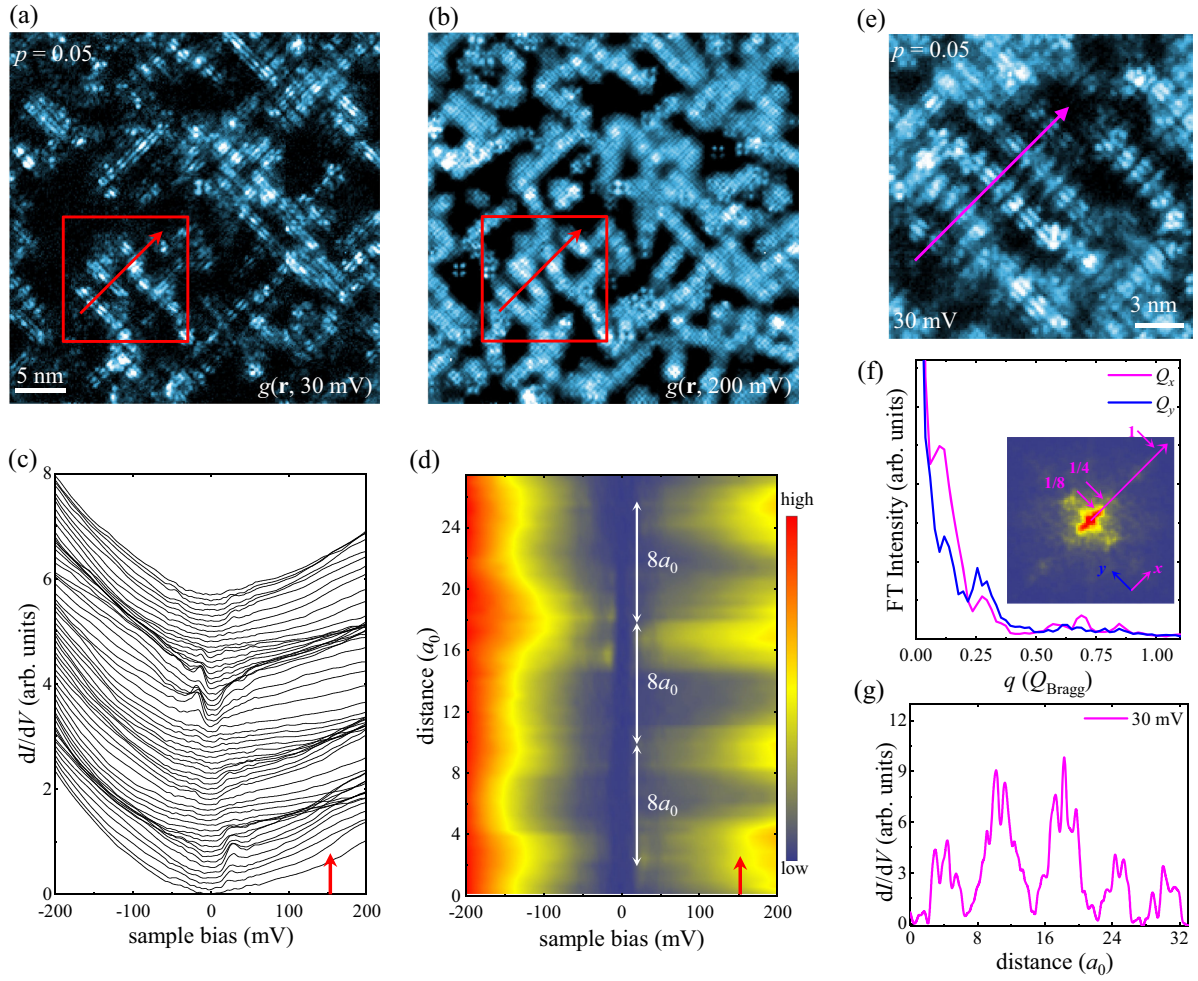



FIG. 2. Eight-unit-cell modulation in the underdoped $p = 0.05$ sample. (a),(b) $\mathrm{d}I/\mathrm{d}V$ maps on the $p = 0.05$ sample at bias $V_\mathrm{b} = 30$ and 200 mV acquired at $T = 5$ K, revealing the formation of molecular orbitals with energy-dependent internal structures. The red square region highlights chainlike assemblies of $4a_0$ plaquettes separated by intervals of approximately $4a_0$. (c),(d) $\mathrm{d}I/\mathrm{d}V$ spectra and corresponding color plot along the red arrow, exhibiting an $8a_0$ modulation over three periods. (e) $\mathrm{d}I/\mathrm{d}V$ map at bias $V_\mathrm{b} = 30$ mV for another FOV with unidirectional $8a_0$ modulation. (f) FT map (inset) of (e) and its line profiles along the Cu-O bond directions. (g) The magenta linecut revealing the coexistence of the $8a_0$ modulation and $1.3a_0$ spacing of internal stripes.

Because the average spacing between internal stripes within a plaquette is around $1.3a_0$ [18,35], the $8a_0$ and $1.3a_0$ modulations should exhibit strong positive correlations along parallel directions and much weaker correlations along perpendicular directions. This is evidenced in both the superconducting and insulating samples in Supplemental Material Sec. VII [19]. These spatial correlations provide a unified description of how the molecular orbital framework emerges from $4a_0$ building blocks with well-defined internal structure.

The progression from $4a_0$ plaquettes to $8a_0$ spatial modulations becomes especially apparent when comparing the $p = 0.05$ data with that on a more dilute $p = 0.03$ sample. Figure 3(a) shows topography of a $p = 0.03$ sample acquired at 23 K. The sparse dopant distribution leads to relatively isolated electronic states and short chains composed of only few $4a_0$ plaquettes, as shown in the $\mathrm{d}I/\mathrm{d}V$ map at 25 mV [Fig. 3(b)] and a typical linecut along the short chain [Fig. 3(c)]. At this low doping level, it is difficult to find neighboring chains with $8a_0$ separation. Figures 3(d) and 3(e) display the topography and $\mathrm{d}I/\mathrm{d}V$ map at another FOV of the same sample with a slightly higher local density of $4a_0$ plaquettes, and Fig. 3(f) is the cut along the red line through clustered plaquettes. The schematic illustrations in Figs. 3(g)–3(j) clarify this real-space picture. A simple chain of adjacent $4a_0$ plaquettes gives rise to a $4a_0$ real-space modulation shown in Figs. 3(g) and 3(h). When $4a_0$ plaquettes alternate with $4a_0$ dark pits, the resulting plaquette–dark pit–plaquette sequence generates an emergent $8a_0$ modulation [Figs. 3(i) and 3(j)]. These data reveal the emergence of spatial separation of approximately $8a_0$ and the correlation with internal stripe patterns, which represents the genesis of $8a_0$ modulation upon doping the parent Mott insulator.

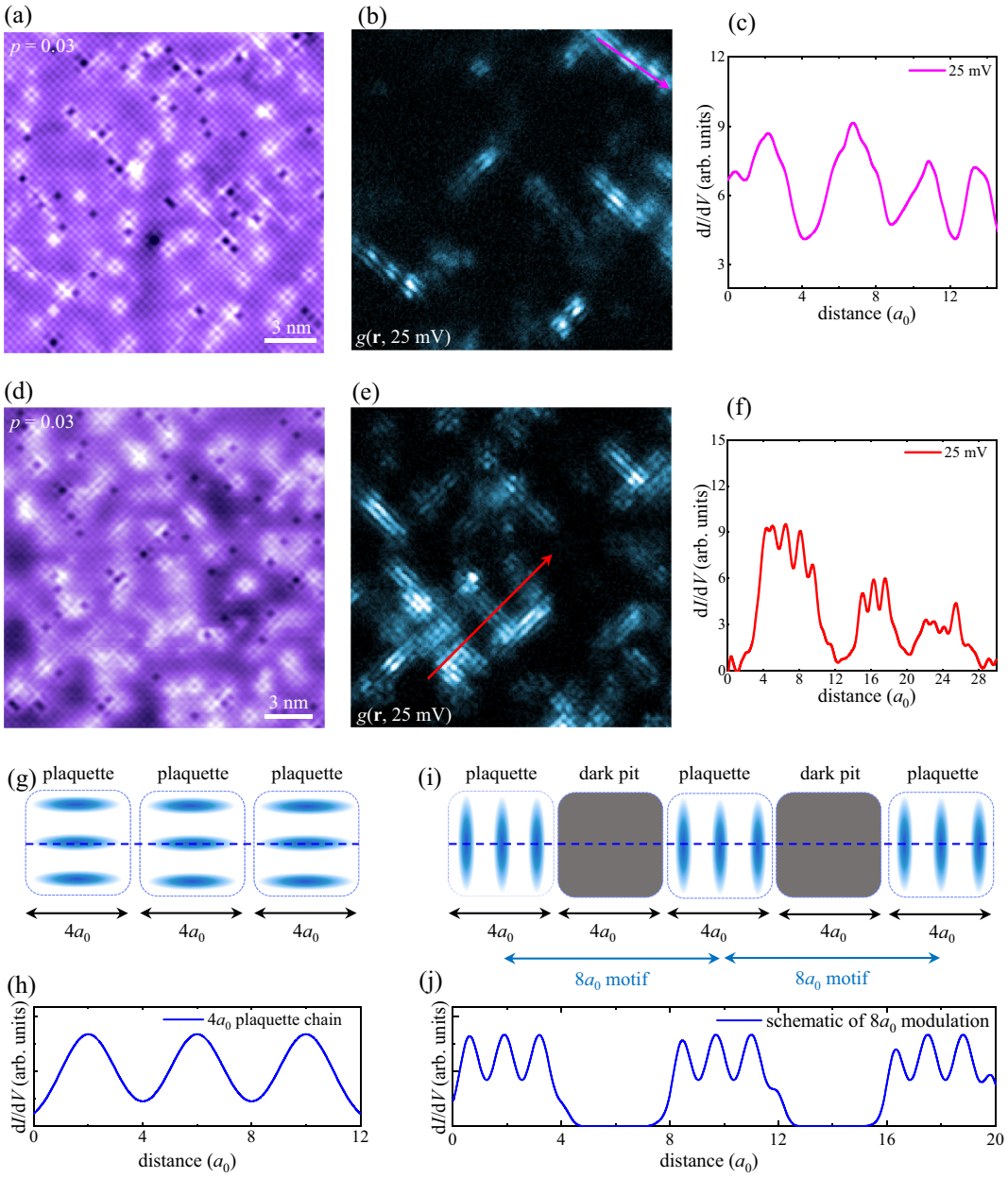



FIG. 3. From $4a_0$ plaquette formation to $8a_0$ real-space modulation via plaquette-pit alternation in the $p = 0.03$ sample. (a) Topographic image of $p = 0.03$ sample acquired at $T = 23$ K. (b) $dI/dV$ map at bias $V_b = 25$ mV, showing the formation of almost isolated plaquettes and short chains. (c) Linecut along the magenta arrow in (b), revealing the formation of $4a_0$ plaquette. (d), (e) Similar dataset as (a) and (b) at another FOV of the same sample with slightly higher local dopant concentration. (f) Linecut along the red arrow in (e), revealing the emergence of $8a_0$ modulation and the internal stripes of the $4a_0$ plaquettes. (g) Schematic representation of a plaquette chain formed by $4a_0$ molecular-orbital plaquettes. (h) Schematic spatial profile along the broken line in (g) corresponding to the $4a_0$ periodicity. (i) Real-space plaquette—dark pit—plaquette sequence illustrating the emergence of $8a_0$ modulation from the alternating $4a_0$ plaquettes and $4a_0$ dark pits. (j) Schematic spatial profile along the broken line in (i) corresponding to the emergent $8a_0$ modulations.

With increasing hole concentration, the plaquettes progressively assemble into extended molecular-orbital network, giving rise to longer range modulations.

To support our picture for the formation of $8a_0$ modulation, we construct a minimal model based on hard-core $4a_0$ plaquettes and study it using the Markov chain Monte Carlo method [42], as described in Supplemental Material Sec. VIII [19]. Figure 4 presents the simulation results for two representative doping levels $p = 0.05$ and 0.10, corresponding to the two samples studied experimentally. For $p = 0.05$, the simulated electronic potential shown in Fig. 4(a) exhibits randomly distributed bright

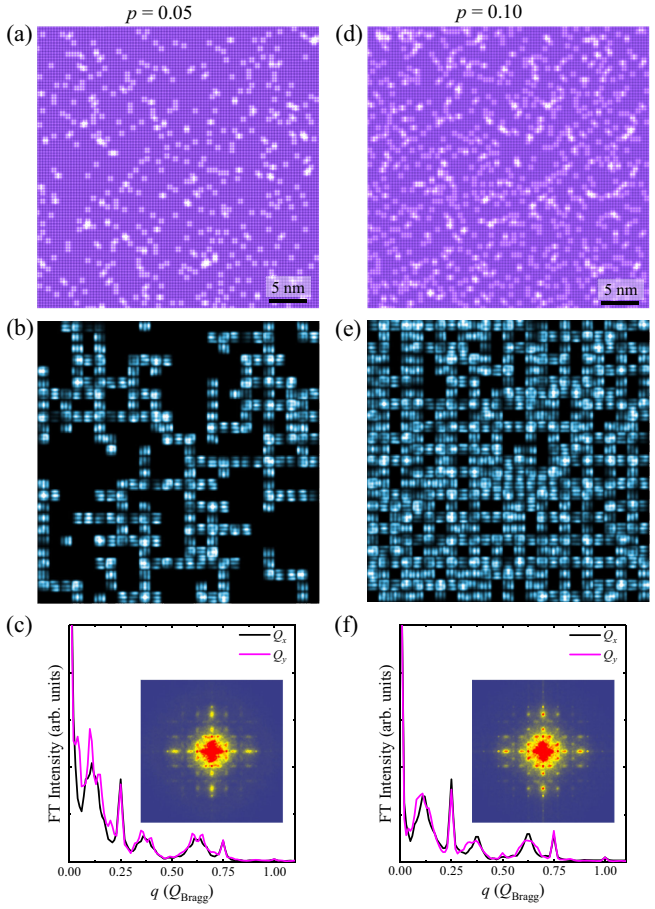



FIG. 4. Monte Carlo simulation illustrating the emergence of $8a_0$ modulations from the self-organization of $4a_0$ molecular orbitals. (a) Impurity potential generated by randomly distributed dopants for $p = 0.05$. (b) Representative low-temperature configurations of $4a_0$ plaquettes, showing the formation of plaquette chains. (c) The line profiles along the corresponding FT (inset), revealing the dominant $4a_0$ periodicity and the accompanying $8a_0$ modulation. (d)–(f) The same set of results as in (a)–(c) for $p = 0.10$. The plaquette chains become longer because of the increased coverage of molecular orbitals. Both the $4a_0$ and $8a_0$ periodicities are clearly observed.

spots, mimicking the local disorder potential induced by dopants. The close resemblance between this simulated landscape and the experimental topography supports the realism of the model. The density of states map obtained from $4a_0 \times 4a_0$ plaquettes after reaching equilibrium is shown in Fig. 4(b), where the plaquettes form short chains along either horizontal or vertical orientation. The line profiles along the corresponding FT map in Fig. 4(c) show a peak at $q$ slightly smaller than $1/8$. This feature originates from the sparse distribution of plaquette chains and is consistent with experimental observations (Fig. 2). Figures 4(d)–4(f) show the corresponding results for $p = 0.10$, with well-defined Fourier peaks at both $q = 1/4$ and $q = 1/8$. As the $4a_0$ plaquettes occupy a larger fraction of the surface, the $1/4$ FT peak becomes more pronounced. At the same time, the relative intensity of the $q = 1/8$ peak is reduced, reflecting the decreased number of $4a_0$ dark pits in this higher doped regime. This comparison illustrates that the strength of the $8a_0$ modulation is primarily determined by the spatial distribution of dark pits. In the lightly doped $p = 0.05$ sample, there are abundant dark pits to generate the $8a_0$ modulation. By contrast, the higher doped $p = 0.10$ sample is more densely occupied by plaquettes with much fewer dark pits, leading to much less $8a_0$ modulation.

Both the experiments and simulations illustrate the assembly of $4a_0 \times 4a_0$ plaquettes into extended chains with increasing hole density. Crucially, when two adjacent chains are bridged by intermediate plaquettes, the empty channel between them is around $4a_0$ wide. Combined with the characteristic $4a_0$ width of each chain, this configuration naturally leads to an $8a_0$ spatial modulation. Upon further doping into the superconducting regime, dark pits with a typical size around $4a_0$ remain, which generate short-range modulations with approximately $8a_0$ separation. The presence of $8a_0$ modulation in both the superconducting and insulating samples, and its persistence across a wide energy range, indicates that it is not directly tied to superconductivity. Nevertheless, it contains the periodic modulations of superconducting properties at sufficiently high doping, so the PDW state can be viewed as a subset of the more inclusive $8a_0$ electronic modulations. In Supplemental Material Sec. IX [19], we show that similar results are also observed in Bi-2212, although the features are weaker than those in CCOC due to more complex structural and dopant properties.

The scenario revealed here is fundamentally different from the conventional PDW picture. First, it has a pure real-space origin stemming from the self-organization of molecular orbitals of doped holes, rather than the $k$ space picture for finite momentum pairing. The $8a_0$ modulations can be clearly pinpointed in the $\mathrm{d}I/\mathrm{d}V$ maps, and the local unidirectional pattern is a natural consequence of the internal structure of molecular orbitals. Second, the $4a_0$ plaquette is the primary entity that emerges earlier in the phase diagram and gives birth to the $8a_0$ modulation. This contrasts sharply with proposals that the $8a_0$ PDW is the primary order that yields the subsidiary $4a_0$ charge order.

In conclusion, we demonstrate that the $8a_0$ electronic modulation in cuprates is the spatial subharmonic of the molecular-orbital patterns with $4a_0 \times 4a_0$ basic units. These results indicate that the $4a_0$ molecular plaquette containing approximately two holes constitutes the elementary building block for the intertwined orders in cuprates. Elucidating the nature of the molecular orbital and its impact on the phase diagram thus represents the most crucial task in solving the mechanism of superconductivity in cuprates.

*Acknowledgments*—Y. W. is supported by the Basic Science Center Project of NSFC (No. 52388201),

Quantum Science and Technology-National Science and Technology Major Project (Grant No. 2021ZD0302502), the CAS Superconducting Research Project (Grant No. SCZX-0101), the Fundamental and Interdisciplinary Disciplines Breakthrough Plan of the Ministry of Education of China (Grant No. JYB2025XDXM112), and the New Cornerstone Science Foundation through the New Cornerstone Investigator Program and the XPLORER PRIZE. S. Y. is supported by NSFC (Grant No. 12475022) and the Quantum Science and Technology—National Science and Technology Major Project (Grant No. 2021ZD0302100). The work at I. O. P. was supported by NSFC (Grant No. 12204515), the National Key Research and Development Program of China (Grants No. 2022YFA1403804 and No. 2023YFA1406001), and the Young Elite Scientists Sponsorship Program of CAST (Grant No. 2022QNRC001).

*Data availability*—All raw and derived data used to support the findings of this work are available from the authors on request.

[1] E. Berg, E. Fradkin, S. A. Kivelson, and J. M. Tranquada, Striped superconductors: How spin, charge and superconducting orders intertwine in the cuprates, New J. Phys. **11**, 115004 (2009).

[2] E. Fradkin, S. A. Kivelson, and J. M. Tranquada, Colloquium: Theory of intertwined orders in high temperature superconductors, Rev. Mod. Phys. **87**, 457 (2015).

[3] D. F. Agterberg, J. C. S. Davis, S. D. Edkins, E. Fradkin, D. J. Van Harlingen, S. A. Kivelson, P. A. Lee, L. Radzihovsky, J. M. Tranquada, and Y. Wang, The physics of pair-density waves: Cuprate superconductors and beyond, Annu. Rev. Condens. Matter Phys. **11**, 231 (2020).

[4] E. Berg, E. Fradkin, and S. A. Kivelson, Theory of the striped superconductor, Phys. Rev. B **79**, 064515 (2009).

[5] E. Berg, E. Fradkin, and S. A. Kivelson, Pair-density-wave correlations in the Kondo-Heisenberg model, Phys. Rev. Lett. **105**, 146403 (2010).

[6] P. A. Lee, Amperean pairing and the pseudogap phase of cuprate superconductors, Phys. Rev. X **4**, 031017 (2014).

[7] E. Berg, E. Fradkin, E.-A. Kim, S. A. Kivelson, V. Oganesyan, J. M. Tranquada, and S. C. Zhang, Dynamical layer decoupling in a stripe-ordered high-$T_c$ superconductor, Phys. Rev. Lett. **99**, 127003 (2007).

[8] Q. Li, M. Hücker, G. D. Gu, A. M. Tsvelik, and J. M. Tranquada, Two-dimensional superconducting fluctuations in stripe-ordered $La_{1.875}Ba_{0.125}CuO_4$, Phys. Rev. Lett. **99**, 067001 (2007).

[9] J. M. Tranquada, B. J. Sternlieb, J. D. Axe, Y. Nakamura, and S. Uchida, Evidence for stripe correlations of spins and holes in copper oxide superconductors, Nature (London) **375**, 561 (1995).

[10] S. Tajima, T. Noda, H. Eisaki, and S. Uchida, *c*-axis optical response in the static stripe ordered phase of the cuprates, Phys. Rev. Lett. **86**, 500 (2001).

[11] M. Hücker, M. V. Zimmermann, G. D. Gu, Z. J. Xu, J. S. Wen, G. Xu, H. J. Kang, A. Zheludev, and J. M. Tranquada, Stripe order in superconducting $La_{2-x}Ba_xCuO_4$ ($0.095 \leqslant x \leqslant 0.155$), Phys. Rev. B **83**, 104506 (2011).

[12] R.-H. He *et al.*, From a single-band metal to a high-temperature superconductor via two thermal phase transitions, Science **331**, 1579 (2011).

[13] M. H. Hamidian *et al.*, Detection of a Cooper-pair density wave in $Bi_2Sr_2CaCu_2O_{8+x}$, Nature (London) **532**, 343 (2016).

[14] W. Ruan, X. Li, C. Hu, Z. Hao, H. Li, P. Cai, X. Zhou, D.-H. Lee, and Y. Wang, Visualization of the periodic modulation of Cooper pairing in a cuprate superconductor, Nat. Phys. **14**, 1178 (2018).

[15] S. D. Edkins *et al.*, Magnetic field–induced pair density wave state in the cuprate vortex halo, Science **364**, 976 (2019).

[16] Z. Du, H. Li, S. H. Joo, E. P. Donoway, J. Lee, J. C. S. Davis, G. Gu, P. D. Johnson, and K. Fujita, Imaging the energy gap modulations of the cuprate pair-density-wave state, Nature (London) **580**, 65 (2020).

[17] X. Li, C. Zou, Y. Ding, H. Yan, S. Ye, H. Li, Z. Hao, L. Zhao, X. Zhou, and Y. Wang, Evolution of charge and pair density modulations in overdoped $Bi_2Sr_2CuO_{6+\delta}$, Phys. Rev. X **11**, 011007 (2021).

[18] S. Ye, J. Zhao, Z. Yao, S. Chen, R. Yu, Z. Dong, Z. Hao, X. Li, L. Shi, Q. Liu, C. Jin, and Y. Wang, Visualization of the Zhang–Rice singlet, electronic molecules and Cooper pair formation in a cuprate superconductor, Nat. Phys. **22**, 1401 (2026).

[19] See Supplemental Material at http://link.aps.org/supplemental/10.1103/lvpn-gblk for details of the experimental methods, additional data analysis, and supporting results, which includes Refs. [20–22].

[20] Y. Kohsaka, M. Azuma, I. Yamada, T. Sasagawa, T. Hanaguri, M. Takano, and H. Takagi, Growth of Na-doped $Ca_2CuO_2Cl_2$ single crystals under high pressures of several GPa, J. Am. Chem. Soc. **124**, 12275 (2002).

[21] M. J. Lawler *et al.*, Intra-unit-cell electronic nematicity of the high-Tc copper-oxide pseudogap states, Nature (London) **466**, 347 (2010).

[22] Y. Kohsaka, T. Hanaguri, M. Azuma, M. Takano, J. C. Davis, and H. Takagi, Visualization of the emergence of the pseudogap state and the evolution to superconductivity in a lightly hole-doped Mott insulator, Nat. Phys. **8**, 534 (2012).

[23] C. Ye, P. Cai, R. Yu, X. Zhou, W. Ruan, Q. Liu, C. Jin, and Y. Wang, Visualizing the atomic-scale electronic structure of the $Ca_2CuO_2Cl_2$ Mott insulator, Nat. Commun. **4**, 1365 (2013).

[24] J. W. Alldredge *et al.*, Evolution of the electronic excitation spectrum with strongly diminishing hole density in superconducting $Bi_2Sr_2CaCu_2O_{8+\delta}$, Nat. Phys. **4**, 319 (2008).

[25] T. Hanaguri, C. Lupien, Y. Kohsaka, D.-H. Lee, M. Azuma, M. Takano, H. Takagi, and J. C. Davis, A "checkerboard" electronic crystal state in lightly hole-doped $Ca_{2-x}Na_xCuO_2Cl_2$, Nature (London) **430**, 1001 (2004).

[26] T. Hanaguri, Y. Kohsaka, J. C. Davis, C. Lupien, I. Yamada, M. Azuma, M. Takano, K. Ohishi, M. Ono, and H. Takagi, Quasiparticle interference and superconducting gap in $Ca_{2-x}Na_xCuO_2Cl_2$, Nat. Phys. **3**, 865 (2007).

[27] J. E. Hoffman, E. W. Hudson, K. M. Lang, V. Madhavan, H. Eisaki, S. Uchida, and J. C. Davis, A four unit cell periodic pattern of quasi-particle states surrounding vortex cores in $Bi_2Sr_2CaCu_2O_{8+\delta}$, Science **295**, 466 (2002).

[28] M. Vershinin, S. Misra, S. Ono, Y. Abe, Y. Ando, and A. Yazdani, Local ordering in the pseudogap state of the high-$T_c$ superconductor $Bi_2Sr_2CaCu_2O_{8+\delta}$, Science **303**, 1995 (2004).

[29] Y. Kohsaka *et al.*, An intrinsic bond-centered electronic glass with unidirectional domains in underdoped cuprates, Science **315**, 1380 (2007).

[30] W. D. Wise, M. C. Boyer, K. Chatterjee, T. Kondo, T. Takeuchi, H. Ikuta, Y. Wang, and E. W. Hudson, Charge-density-wave origin of cuprate checkerboard visualized by scanning tunnelling microscopy, Nat. Phys. **4**, 696 (2008).

[31] E. H. Da Silva Neto *et al.*, Ubiquitous interplay between charge ordering and high-temperature superconductivity in cuprates, Science **343**, 393 (2014).

[32] A. Mesaros, K. Fujita, S. D. Edkins, M. H. Hamidian, H. Eisaki, S. Uchida, J. C. S. Davis, M. J. Lawler, and E.-A. Kim, Commensurate $4a_0$-period charge density modulations throughout the $Bi_2Sr_2CaCu_2O_{8+x}$ pseudogap regime, Proc. Natl. Acad. Sci. U.S.A. **113**, 12661 (2016).

[33] P. Cai, W. Ruan, Y. Peng, C. Ye, X. Li, Z. Hao, X. Zhou, D.-H. Lee, and Y. Wang, Visualizing the evolution from the Mott insulator to a charge-ordered insulator in lightly doped cuprates, Nat. Phys. **12**, 1047 (2016).

[34] S. Ye, C. Zou, H. Yan, Y. Ji, M. Xu, Z. Dong, Y. Chen, X. Zhou, and Y. Wang, The emergence of global phase coherence from local pairing in underdoped cuprates, Nat. Phys. **19**, 1301 (2023).

[35] N. Xia, Y. Guo, and S. Yang, Unveiling stripe-shaped charge density modulations in doped Mott insulators, Phys. Rev. Lett. **135**, 116504 (2025).

[36] J. Repp, G. Meyer, S. M. Stojković, A. Gourdon, and C. Joachim, Molecules on insulating films: Scanning-tunneling microscopy imaging of individual molecular orbitals, Phys. Rev. Lett. **94**, 026803 (2005).

[37] E. Sierda, X. Huang, D. I. Badrtdinov, B. Kiraly, E. J. Knol, G. C. Groenenboom, M. I. Katsnelson, M. Rösner, D. Wegner, and A. A. Khajetoorians, Quantum simulator to emulate lower-dimensional molecular structure, Science **380**, 1048 (2023).

[38] K. Fujita *et al.*, Direct phase-sensitive identification of a *d*-form factor density wave in underdoped cuprates, Proc. Natl. Acad. Sci. U.S.A. **111**, E3026 (2014).

[39] R. Comin *et al.*, Symmetry of charge order in cuprates, Nat. Mater. **14**, 796 (2015).

[40] M. H. Hamidian *et al.*, Atomic-scale electronic structure of the cuprate *d*-symmetry form factor density wave state, Nat. Phys. **12**, 150 (2016).

[41] C. McMahon *et al.*, Orbital symmetries of charge density wave order in $YBa_2Cu_3O_{6+x}$, Sci. Adv. **6**, eaay0345 (2020).

[42] W. Krauth, *Statistical Mechanics: Algorithms and Computations* (Oxford University Press, Oxford, 2006).